Int. J. Electrochem. Sci., 14 **(2019)** 4420 – 4442, doi: 10.20964/2019.05.31

International Journal of
ELECTROCHEMICAL
SCIENCE
www.electrochemsci.org

Performance of $(HEMIM)^+ (CN)^-$ and $(DMIM)^+ (Cl)^-$ as corrosion inhibitor of API 5L X52 steel in HCl medium

Mónica Corrales-Luna[1], *Tu Le Manh*[1,2,3], *E.M. Arce-Estrada*[1*]

[1]Instituto Politécnico Nacional. ESIQIE, Departamento de Ingeniería en Metalurgia y Materiales. UPALM, Ed. 7. CDMX, 07738. México.
[2]Faculty of Materials Science and Engineering, Phenikaa Institute for Advanced study (PIAS), Phenikaa University, Hanoi 100000, Vietnam
[3]Phenikaa Research and Technology Institute (PRATI), A&A Green Phoenix Group, 167 Hoang Ngan, Hanoi 10000, Viet Nam
[*]E-mail: earce@ipn.mx

Received: 6 January 2019 / *Accepted:* 27 February 2019 / *Published:* 10 April 2019

Two ionic liquids, 1-(2-hydroxyethyl)-3-methylimidazolium dicyanamide $(HEMIM)^+ (CN)^-$ and 1,3-didecyl-2-methylimidazolium chloride $(DMIM)^+ (Cl)^-$, were evaluated as corrosion inhibitors of the API 5L X52 in 0.5 M HCl using electrochemical method, weight loss, and surface characterization techniques. Gravimetric tests showed that the ILs display high corrosion protection efficiency, % *EI*, (92 % and 97 %) with 100 and 5 ppm of $(HEMIM)^+ (CN)^-$ and $(DMIM)^+ (Cl)^-$, respectively. Electrochemical tests showed that the % *EI* depends on the IL concentration and the temperature. The polarization studies showed that the ILs are mixed type inhibitors and the adsorption of the ILs on the API 5L X52 obeyed the Langmuir adsorption isotherm displaying chemical interaction between the steel and the IL. SEM and AFM verified a considerable reduction of the corrosion process after the addition of the ILs. Uv-vis also confirmed the interaction between ILs and steel. Theoretical quantum chemical calculation studies agree with experimental results. The adsorption energy of $(DMIM)^+ (Cl)^-$ on Fe (110) surface is higher than that of $(HEMIM)^+ (CN)^-$, but both inhibitors are expected to bind strongly to the API 5L X52.

Keywords: Ionic liquid; corrosion inhibitor; API 5L X52 steel; electrochemical tests.

1. INTRODUCTION

There are different methods for corrosion control of metallic structures. Unfortunately, the selection and application of the appropriate method depends on the corrosive environment as well as economic considerations [1]. For decades, the most economical way to control corrosion in petrochemical industry has been the use of corrosion inhibitor (CI), so that, in each stage of the oil production, it is well defined what type of CIs should be used [2]. However, the significant growth in the production of heavy crude brought as a consequence the increase of contaminants that favor the corrosion processes. For this reason, the inhibitors, which are traditionally used to solve the problems caused by corrosion, could be not adequate for these new conditions. Furthermore, the CI must fulfill the environmental regulations established worldwide such as the environmental criteria of toxicity, biodegradability, and bioaccumulation. Therefore, the new investigations are focused on the search for inhibitors that are environmentally friendly and do not present high toxicity [3].

It has been established in the literature [4-6] that the ionic liquids, ILs, have shown good characteristics of corrosion inhibition in acid medium. These compounds are melt at temperatures below 100 °C and are composed of pairs of ions, a cation of organic nature and an anion of organic or inorganic nature. The cation and the anion can be selected in such a way that the resulting salts cannot be easily crystallized so that they remain in the liquid state within a wide range of temperatures. There are many possible combinations that the ILs can be modulated depending on the cation and the anion, which make it. The most common cations are those of imidazolium, pyridinium, ammonium, pyrrolidinium, and phosphonium, while the most common anions are trifluoromethylsulfonylimide, hexafluorophosphate, trifluoromethylsulfonate, and halides [7-13]. However, due to the abundance of the organic compounds, the knowledge on the capacity of the ILs as corrosion inhibitors is not completed.

In the present work, the viability of two molecules of the ILs derived from the imidazolium was studied as corrosion inhibitors of API 5L X52 in HCl medium, using weight loss and electrochemical measurements, spectroscopic methods, and molecular simulation.

2. MATERIALS AND METHODS

2.1 Materials

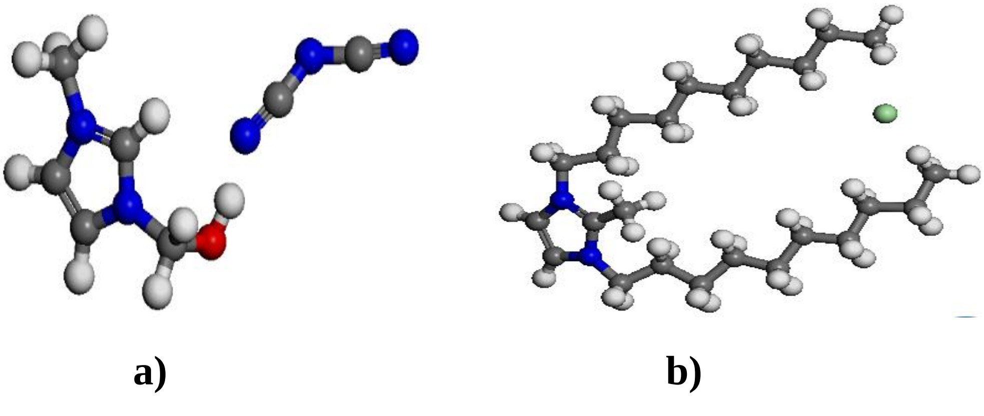

a) **b)**

Figure 1. Chemical structure of a) $(HEMIM)^+ (CN)^-$ and b) $(DMIM)^+ (Cl)^-$ IL as corrosion inhibitor.

The samples for the electrochemical and corrosion tests were obtained from the API 5L X52 pipeline steel with the chemical composition of 0.24 % C, 0.05 % Si, 0.001 % Mo, 0.01 % Cu, 0.021 % Ni, 0.018 % P, 0.014 % S, 0.092 % V, and balanced with Fe. All these samples were abraded with emery papers (320, 400, and 600); and finally, the samples were degreased with acetone to remove any residual impurity on the surface.

Solutions of 0.5 M HCl (Fermont, 37 %) with and without inhibitor were prepared with deionized water. The IL 1-(2-Hydroxyethyl)-3-methylimidazolium dicyanamide $(HEMIM)^+$ $(CN)^-$ (Fluka, 97 %), Figure 1a, and 1,3-Didecyl-2-methylimidazolium chloride $(DMIM)^+$ $(Cl)^-$ (Fluka, 96 %), Figure 1b, were evaluated as corrosion inhibitors. The used inhibitor concentrations were varied between 1-100 ppm.

2.2. Weight loss measurements

Immersion test of cylindrical steel (1.0 × 1.0 × 0.5 cm) was performed by triplicate in 100 ml of 0.5 M HCl, in the absence and presence of varying the ILs concentrations (5 to 100 ppm) during 120 h at room temperature. After that, the corrosion products were removed, dried, and weighed. The initial and final weights of the samples were recorded using an analytical balance (± 0.1 mg).

2.3 Electrochemical measurements

Potentiodynamic polarization and EIS measurements were performed with a conventional water/jacket cell temperature controlled by PolyScience circulator. The electrochemical cell consisted of a three-electrode system: an API 5L X52 steel cylinder encapsulated in epoxy resin with a surface area of 0.1963 cm^2 as the working electrode (WE), a saturated calomel electrode (SCE) coupled to a Luggin capillary (maintaining closed to the WE to minimize the ohmic contribution) as the reference electrode, and a graphite bar as the counter electrode. The electrochemical measurements were carried out using a Potentiostat/Galvanostat Autolab PGSTAT30 at different temperatures (25, 45, 50, 55 °C) using fresh solutions for each one. Each experiment was repeated in triplicate to ensure the reproducibility.

The potentiodynamic polarization curves were performed in the test solution after reaching the open-circuit potential (OCP) in the potential window ranging from -250 to +250 mV vs. the open circuit potential (OCP) with a scan rate of 0.166 mV s^{-1}, 30 minutes needed to stabilize the OCP.

EIS measurements were carried out in triplicate at OCP, in the frequency range from 10 mHz to 100 kHz with an amplitude of 10 mV AC signal.

2.4. Surface morphological analysis

The steel surface features after the immersion tests (24 h) in the acid solution in the presence and absence of the ILs were characterized by scanning electron microscopy, SEM, using JEOL JSM-6701F). The surface roughness was determined by atomic force microscopy, AFM, using NanoScope analysis 1.5 software.

2.5. UV-Visible spectroscopy analysis

UV-Vis spectra measurements were obtained from the pure ILs and 100 ppm of $(HEMIM)^+$ $(CN)^-$ and 5 ppm of $(DMIM)^+$ $(Cl)^-$ solutions where the API 5L X52 steel was immersed for 24 h. Perkin Elmer Lambda 35 UV-Vis spectrophotometer was used in the wavelength region ranging within 200-400 nm.

2.6 Theoretical calculation

The corrosion inhibitor simulations were carried out using Material Studio 6.0 software from Accelrys Inc., USA. Density functional theory, DFT, implemented in Material Studio Package, was applied to analysis the characteristics of the IL/metal surface and predict the molecular reactivity descriptors such as the highest occupied molecular orbital (HOMO), the lower unoccupied molecular orbital (LUMO), the energy difference between HOMO and LUMO (ΔE = (HOMO – LUMO) energy gap) [24]. These parameters are directly involved in the inhibitive properties of the molecule adsorbed on the metal surface. On the other hand, the molecular dynamics simulation, MD, can offer information about the adsorption energy, which describes the interaction between the metal plane surface and the inhibitor molecules, associated with the IL inhibition capacity. Chemical parameters such as electron affinity (A), ionization potential (I), dipole moment (μ), hardness (η), and softness (σ) were determined from simulations using the following expressions:

$$A = -E_{LUMO} \tag{1}$$

$$I = -E_{HOMO} \tag{2}$$

$$\eta = \frac{(I-A)}{2} \tag{3}$$

$$\sigma = \frac{1}{\gamma} \tag{4}$$

3. RESULTS AND DISCUSSION

3.1. Weight loss

Using the weight loss technique, the inhibition efficiency, % EI_{WL}, of the two ILs on API 5L X52 steel immersed for 120 h in a 0.5 M HCl solution was evaluated in the absence and presence of different ILs concentrations (1 to 100 ppm) at 25 °C. The corrosion rate, v_{corr}, values were calculated from equation (5):

$$v_{corr} = \frac{(W_1 - W_2)}{S\,X\,t} \tag{5}$$

where W_1 and W_2 are the weights of the samples before and after immersion in the corrosive medium, respectively, S is the area of the sample and t is the immersion time. From these data, the $\% EI_{WL}$ was determined by:

$$\% EI_{WL} = \frac{v_{corr}^{blanco} - v_{corr}^{IL}}{v_{corr}^{IL}} \times 100 \tag{6}$$

where v_{corr}^{blanco} and v_{corr}^{IL} are the corrosion current density values in the presence and absence of inhibitor, respectively.

Figure 2 shows the comparison between the variation of the % EI_{WL} and the vcorr as a function of the concentration of the ILs studied, observing in both cases an increase in the % EI_{WL} and a decrease in the v_{corr} with the gradual rise in the ILs concentration. These results indicate that the ILs adsorption on the steel surface increases with the increase of their concentration and that the formed film acts as an insulator between the steel and the aggressive medium to decrease the corrosion process. However, it is important to note that in the case of $(HEMIM)^+$ $(CN)^-$ to obtain an efficiency of 92 %, the addition of

100 ppm was required, while for $(DMIM)^+$ $(Cl)^-$ only 5 ppm was required to achieve an efficiency of 97 %, see Table 1.

This higher efficiency can be explained by the fact that the length of the chain $(DMIM)^+$ $(Cl)^-$ provides greater coverage of the surface of the steel.

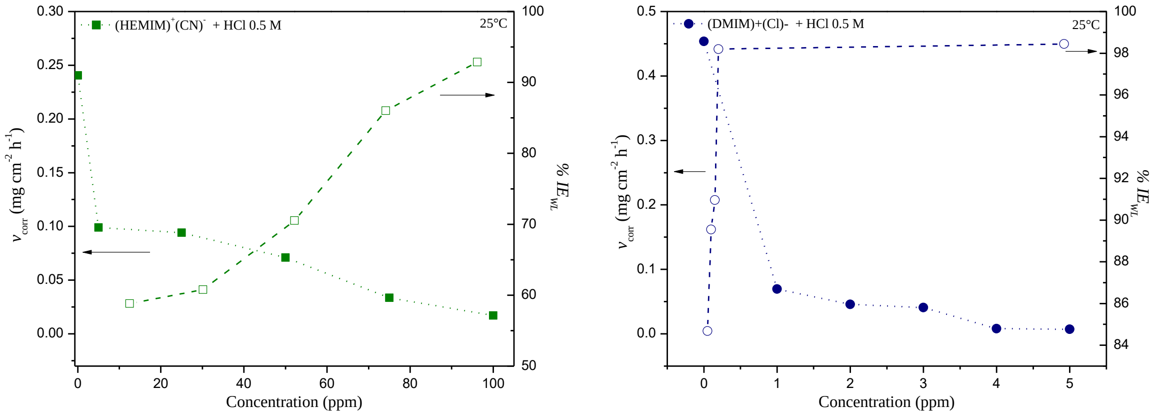

a) **b)**

Figure 2. Variation of corrosion rate and inhibition efficiency of API 5L X52 steel in the presence and absence of different concentrations of a) $(HEMIM)^+$ $(CN)^-$ and b) $(DMIM)^+$ $(Cl)^-$ in 0.5 M HCl obtained for weight loss.

Table 1. Corrosion rate and inhibition efficiency of API 5L X52 in 0.5 M HCl in the presence of $(HEMIM)^+$ $(CN)^-$ and $(DMIM)^+$ $(Cl)^-$ determined by immersion for 120 h at 25 °C obtained by the loss weight.

Inhibitor	Concentration (ppm)	v_{corr} (mg cm^{-2} h^{-1})	IE_{WL} (%)
$(HEMIM)^+$ $(CN)^-$	Blank	0.2405 ± 0.06	-
	5	0.0990 ± 0.03	58.8 ± 0.03
	25	0.0942 ± 0.03	60.7 ± 0.03
	50	0.0709 ± 0.01	70.5 ± 0.01
	75	0.0335 ± 0.01	86.0 ± 0.01
	100	0.0171 ± 0.02	92.8 ± 0.02
$(DMIM)^+$ $(Cl)^-$	Blank	0.2405 ± 0.06	-
	1	0.0694 ± 0.02	71.1 ± 0.02
	2	0.0457 ± 0.03	80.9 ± 0.03
	3	0.0409 ± 0.02	82.9 ± 0.02
	4	0.0081 ± 0.01	96.6 ± 0.01
	5	0.0070 ± 0.01	97.1 ± 0.02

3.2 Electrochemical measurements

3.2.1 Potentiodynamic polarization

Figure 3 shows the potentiodynamic polarization curves obtained for API 5L X52 steel immersed in a 0.5 M HCl solution in the absence and presence of different concentrations of the ILs (1 to 100 ppm) obtained at a sweep rate of 0.166 mV s^{-1} and a temperature of 25 ± 1 °C. The cathodic and anodic branches obtained for the (HEMIM)$^+$ (CN)$^-$ show a typical Tafel behavior. However, for the (DMIM)$^+$ (Cl)$^-$ it is only satisfied in a decade, so the kinetic parameters in both cases were acquired by extrapolation of both branches using the Nova 1.11 software. The corrosion potential (E_{corr}), anodic and cathodic slopes (β_a and β_c) and the corrosion current density (j_{corr}) values are shown in Tables 2 and 3. The % EI_{PP} was calculated by the following equation [14].

$$\% \, EI_{PP} = \frac{j_{corr}^{blank} - j_{corr}^{IL}}{j_{corr}^{blank}} \times 100 \qquad (7)$$

where $j_{\mathrm{corr}}^{\mathrm{blank}}$ and $j_{\mathrm{corr}}^{\mathrm{IL}}$ are the corrosion current density values in presence and absence of inhibitor, respectively.

It is evident in Figure 3b the presence of a defect (kink) in the anodic polarization curve when the IL is present, that could be associated with changes in the degree of coating as a consequence of the reorientation of the heteroatoms of the IL cation or to the release of corrosion products formed on the steel surface [15]. A displacement of the polarization curves towards lower values of current in the presence of the IL is also observed. In the case of (HEMIM)$^+$ (CN)$^-$ (Figure 3a) the displacement in the anodic branch is evident. However, this does not change with the increase in the IL concentration. Nevertheless, the cathodic branch shows a displacement with the increase of the IL concentration.

Meanwhile, for the (DMIM)$^+$ (Cl$^{)-}$ (Figure 3b) both branches move towards lower values of current density with the increase in the IL concentration. This behavior indicates that both IL are mixed type inhibitors because they suppress both reactions, the oxidation of steel and the evolution of hydrogen. The $j - E$ plots are similar in the absence and presence of the IL, showing that the IL addition does not modify the reaction mechanism, but only block the active sites [16].

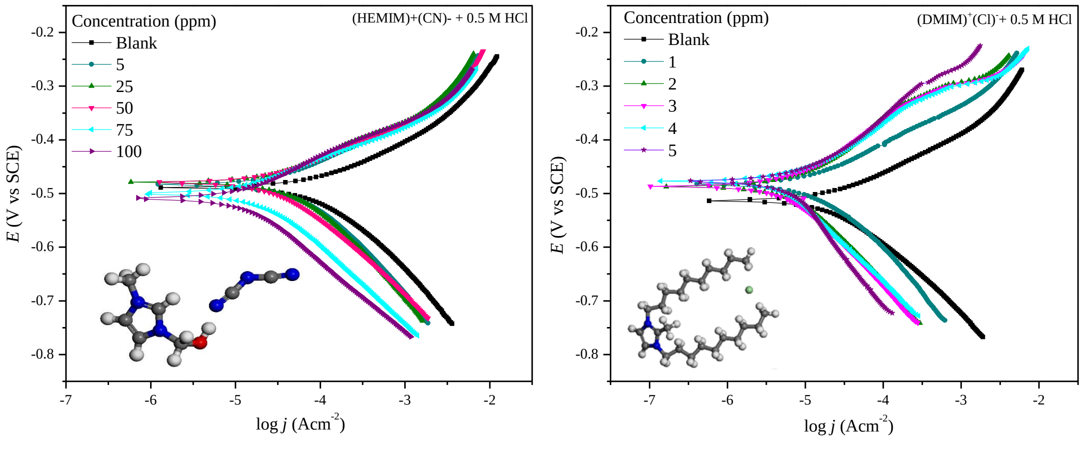

a) **b)**

Figure 3. Polarization curves of API 5L X52 steel in 0.5 M HCl in the absence and presence of different concentrations of a) (HEMIM)$^+$ (CN)$^-$ and b) (DMIM)$^+$ (Cl)$^-$ at 25 °C and v = 0.166 mV s^{-1} .

The study of the temperature effect on the corrosion inhibition reactions is very complex because various changes occur in the metal surface, such as the increase in the corrosion rate, the adsorption/desorption of the CI or its decomposition [17]. Therefore, it is important to establish its effect on the corrosion process. The kinetic parameters obtained in the absence and presence of the ILs at 25, 45, 50, and 55 °C are shown in Tables 2 and 3. It can be observed that the j_{corr} values decrease with the increase in the concentration for both compounds at 25 °C. % IE_{PP} of 83.2 % for the $(HEMIM)^+$ $(CN)^-$ and 90.9 % for $(DMIM)^+$ $(Cl)^-$ in the presence of 100 and 5 ppm, respectively were obtained. However, with the increase in temperature, $(HEMIM)^+$ $(CN)^-$ loses its inhibition effect, especially at low concentrations. In the case of $(DMIM)^+$ $(Cl)^-$ the efficiencies decrease at 45 and 55 °C for 1 and 3 ppm, but in the presence of 4 and 5 ppm, the efficiency is increased to 90 %.

Table 2. Electrochemical parameters obtained from the potentiodynamic polarization curves of API 5L X52 steel in 0.5 M HCl in the absence and presence of varying $(HEMIM)^+$ $(CN)^-$ concentrations at different temperatures.

Temperature (°C)	Concentration (ppm)	β_a (mV dec^{-1})	-β_c (mV dec^{-1})	-E_{corr} (mV/SCE)	j_{corr} (µA cm^{-2})	IE_{PP} (%)
25	Blank	140	77	487	453	-
	5	142	92	482	243	46.3 ± 0.04
	25	140	94	479	209	53.8 ± 0.06
	50	127	78	478	143	68.4 ± 0.06
	75	125	79	501	78	82.7 ± 0.05
	100	141	94	507	76	83.2 ± 0.03
45	Blank	184	81	478	764	-
	5	144	96	460	700	8.4 ± 0.09
	25	138	72	445	630	17.5 ± 0.08
	50	149	83	446	625	18.2 ± 0.07
	75	137	74	431	508	33.4 ± 0.07
	100	140	75	430	205	73.1 ± 0.07
50	Blank	171	79	477	995	-
	5	151	90	450	1090	-
	25	174	90	442	887	10.8 ± 0.08
	50	139	78	437	863	13.2 ± 0.06
	75	154	76	461	649	34.7 ± 0.03
	100	125	84	482	262	73.6 ± 0.01
55	Blank	112	98	478	843	-
	5	144	75	433	380	54.9 ± 0.2
	25	159	113	436	357	57.6 ± 0.1
	50	133	80	445	341	59.5 ± 0.1
	75	144	95	459	235	72.1 ± 0.2
	100	124	69	446	170	79.8 ± 0.1

Tabla 3. Electrochemical parameters obtained from the potentiodynamic polarization curves of API 5L X52 steel in 0.5 M HCl in the absence and presence of varying concentrations of (DMIM)$^+$ (Cl)$^-$ at different temperatures.

Temperature (°C)	Concentration (ppm)	β_a (mVdec^{-1})	$-\beta_c$ (mVdec^{-1})	$-E_{corr}$ (mV/SCE)	j_{corr} (µA cm^{-2})	IE_{PP} (%)
25	Blank	140	78	513	453	-
	1	140	86	482	72	84.1 ± 0.02
	2	139	115	479	56	87.6 ± 0.01
	3	188	121	486	50	88.9 ± 0.02
	4	191	113	476	42	90.7 ± 0.02
	5	191	104	477	41	90.9 ± 0.03
45	Blank	184	81	478	764	-
	1	117	92	466	353	53.8 ± 0.02
	2	122	115	464	277	63.7 ± 0.01
	3	121	97	478	235	69.2 ± 0.02
	4	137	126	452	83	89.1 ± 0.02
	5	132	112	482	81	89.4 ± 0.01
50	Blank	171	79	477	995	-
	1	140	120	470	592	40.5 ± 0.02
	2	118	134	472	531	46.6 ± 0.02
	3	134	132	483	237	76.1 ± 0.01
	4	122	134	477	154	84.5 ± 0.03
	5	134	122	455	73	92.6 ± 0.01
55	Blank	112	86	478	843	
	1	140	189	492	431	48.8 ±0.03
	2	137	163	472	371	55.9 ±0.03
	3	130	172	512	329	60.9 ±0.03
	4	133	141	486	180	78.6 ± 0.03
	5	129	133	453	83	90.1 ± 0.02

3.2.2 Electrochemical impedance spectroscopy (EIS)

EIS is widely used for the study of metal/solution interfaces since it allows to establish the different contributions and inhibition mode of the studied inhibitor. Figure 4 displays the Nyquist and Bode diagrams obtained for API 5L X52 steel in 0.5 M HCl in the absence and presence of (HEMIM)$^+$ (CN)$^-$ and (DMIM)$^+$ (Cl)$^-$ at OCP and 25 °C, using the frequency range between 10 mHz to 100 kHz. In all cases, the typical corrosion behavior of steel in an acid medium, a capacitive semicircle, is observed. Nyquist and Bode diagrams in the presence of IL are similar to those obtained in their absence, indicating that the corrosion mechanism is not modified but its kinetics, due to the IL adsorption on the active sites of the steel surface [18].

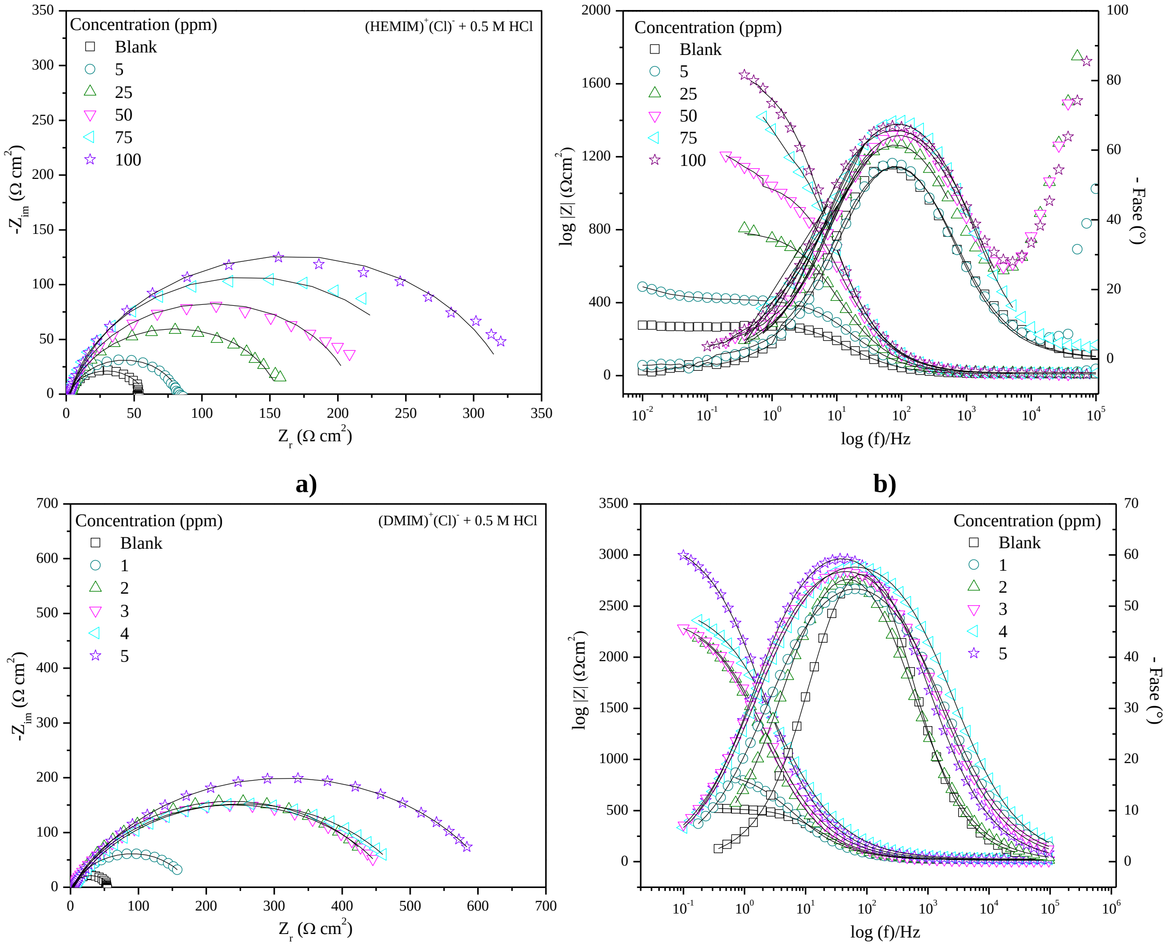

a)

b)

c)

d)

Figure 4. Nyquist plots of API 5L X52 steel in 0.5 M HCl and different concentrations of a) (HEMIM)$^+$ (CN)$^-$ and b) (DMIM)$^+$ (Cl)$^-$, at 25 °C.

It is evident that in the Nyquist diagrams, the semicircle diameter increases gradually with the increase in the IL concentrations; this behavior has been associated with the charge transfer resistance (R_{ct}). This resistance is inversely proportional to the corrosion rate in processes under kinetic control. The increase in the R_{ct} is due to the greater adsorption of IL molecules on the steel surface, which reduces the transport of chemical species through the metal interface and the v_{corr} accordingly. Figure 4 shows that in the absence of inhibitor the R_{ct} has a value of 56.5 Ω cm^2, signifying that the current density and corrosion rate associated with corrosion process are high because, although the formation of corrosion products generates a certain R_{ct}, it does not effectively decrease the metal corrosion. [19]. The R_{ct} values rise with the increase in the IL concentration, for the sake of example: with an addition of 100 and 5 ppm it takes values of 329.8 Ω cm^2 and 626.1 Ω cm^2 for the (HEMIM)$^+$ (CN)$^-$ and (DMIM)$^+$ (Cl)$^-$, respectively, confirming the significant role of the inhibitor in the prevention of corrosive processes and better efficiency of the (DMIM)$^+$ (Cl)$^-$. Bode diagrams also confirm greater protection for higher concentrations, since the phase-angle values are observed to be increased with the gradual variations of the IL concentration [20].

Figure 5 shows the equivalent circuit with a time constant that is frequently used to analyze the uniform corrosion of the steel, which consists of a resistance of the solution (R_s), a constant phase element associated with the capacitance of the double layer (CPE_{dl}) and a charge transfer resistance (R_{ct}). The experimental data were fitted with the EIS Analyzer software. Figure 4 shows the fitted data by the solid lines, and it is observed a satisfactory agreement with the experimental data (symbols).

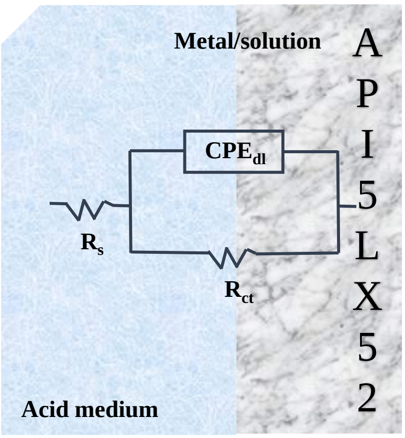

Figure 5. Equivalent electric circuit.

In the proposed circuit to carry out the adjustment, the CPE_{dl} was introduced to represent the non-ideality of the double layer due to the roughness, impurities, dislocations, grain limit, distribution of the active sites, and adsorption of the inhibitor [21] that may be presented in the system. The impedance of the CPE_{dl} is defined as follows [22]:

$$Z(CPE) = Y_0^{-1}(j\omega)^{-n} \qquad (8)$$

where Y_0 is the magnitude of the CPE_{dl}, ω is the angular frequency (rad s^{-1}), $j^2 = -1$ is the imaginary number and n is the exponent of the CPE, which considers the degree of non-ideality of the surface. The value of n could be associated with the surface heterogeneity, taking values from 0 to 1. If $n = 0$ the behavior corresponds to a resistance, $n = 1$ corresponds to a capacitance, $n = -1$ corresponds to an inductance, and if $n = 0.5$ it corresponds to a Warburg. [23].

The double electric layer between the charged metal surface and the solution can be considered as a capacitor, due to its electrical characteristics. The values of the capacitance of the double layer, C_{dl}, associated with CPE_{dl}, were calculated from the following equation [24]:

$$C_{dl} = (Y_0\, R_{ct}^{1-n})^{1/n} \qquad (9)$$

Table 4 and 5 show the values obtained from the fitting. It is observed that the R_{ct} increases and that simultaneously the values of the C_{dl} decrease with the increase in the concentration of the IL, confirming the inhibition efficiency of the IL. The decrease in the values of the C_{dl} can be attributed to the decrease in the dielectric constant due to greater adsorption of the ILs as the concentration or the thickness of the double layer increases, or both of them [25].

Table 4. Electrochemical parameters obtained by EIS measurements for API 5L X52 steel in 0.5 M HCl in the absence and presence of $(HEMIM)^+ (CN)^-$ at different temperatures.

Temperature (°C)	Concentration (ppm)	R_s (Ω cm^2)	C_{dl} (μF cm^2)	*n*	R_{tc} (Ω cm^2)	IE_{EIS} (%)
25	Blank	1.96	278	0.83	56.5	-
	5	3.17	170	0.84	79.7	31.3 ± 0.01
	25	1.74	144	0.84	154.1	64.5 ± 0.02
	50	2.81	104	0.85	209.3	73.9 ± 0.01
	75	2.62	96	0.87	262.0	79.1 ± 0.03
	100	2.66	108	0.84	329.8	83.4 ± 0.03
45	Blank	2.96	175	0.84	51.6	-
	1	2.01	160	0.84	44.7	-
	2	2.08	206	0.84	47.5	-
	3	2.18	197	0.82	48.4	-
	4	3.32	78	0.83	180.6	71.4 ± 0.05
	5	3.05	84	0.81	190.5	72.9 ± 0.04
50	Blank	1.35	232	0.84	24.9	-
	1	2.39	274	0.86	25.7	3.3 ± 0.06
	2	2.00	235	0.84	26.8	7.2 ± 0.04
	3	2.37	130	0.87	36.7	32.2 ± 0.04
	4	2.42	202	0.82	52.0	52.1 ± 0.05
	5	2.19	258	0.84	53.6	53.6 ± 0.06
55	Blank	1.73	105	0.85	50.9	-
	1	1.89	200	0.84	48.5	-
	2	2.14	106	0.86	54.4	6.34 ± 0.05
	3	1.83	129	0.83	57.9	12.15 ± 0.06
	4	2.78	107	0.86	109.7	53.6 ± 0.06
	5	2.12	99	0.88	127.6	60.1 ± 0.04

Table 5. Electrochemical parameters obtained by EIS measurements for API 5L X52 steel in 0.5 M HCl in the absence and presence of $(DMIM)^+ (Cl)^-$ at different temperatures.

Temperature (°C)	Concentration (ppm)	R_s (Ω cm^2)	C_{dl} (μF cm^2)	n	R_{tc} (Ω cm^2)	IE_{EIS} (%)
25	Blank	1.96	278	0.83	56.5	-
	1	4.04	209	0.79	172.4	68.3 ± 0.02
	2	3.25	237	0.75	466.9	88.3 ± 0.03
	3	2.34	211	0.72	475.4	88.5 ± 0.02
	4	4.97	132	0.70	495.8	89.0 ± 0.05
	5	4.17	182	0.72	626.1	91.3 ± 0.03
45	Blank	2.96	175	0.84	51.6	-
	1	1.70	146	0.74	157.7	82.5± 0.02
	2	1.84	206	0.71	170.1	83.8± 0.03
	3	1.99	161	0.71	266.7	89.7± 0.02
	4	2.65	91	0.74	285.8	90.3± 0.04
	5	2.64	98	0.72	401.4	93.1± 0.03
50	Blank	1.35	232	0.84	24.9	-
	1	1.86	269	0.75	62.3	60.0± 0.02
	2	1.66	168	0.78	89.1	72.1± 0.03
	3	1.67	174	0.72	139.3	82.1± 0.02
	4	1.84	145	0.70	178.6	86.0± 0.05
	5	2.34	107	0.72	408.8	93.9± 0.03
55	Blank	1.73	105	0.85	50.9	-
	1	1.55	159	0.80	69.7	26.9± 0.02
	2	1.45	184	0.71	132.3	61.5± 0.03
	3	1.79	134	0.74	168.5	69.8± 0.02
	4	2.17	146	0.76	176.2	71.1± 0.05
	5	2.08	225	0.72	353.4	85.6± 0.03

The values of n in the absence and presence of the inhibitor are in the order of 0.80, indicating that the homogeneity of the surface is not modified by the presence of the IL. The % EI_{EIS} values are consistent with the results previously obtained by weight loss and potentiodynamic polarization methods (see Tables 1 to 3). Therefore, the best inhibition efficiency corresponds to the presence of 100 ppm of the $(HEMIM)^+ (CN)^-$ and 5 ppm of the $(DMIM)^+ (Cl)^-$ at 25 °C, respectively.

3.3 Surface analysis

3.3.1 Scanning electron microscopy (SEM)

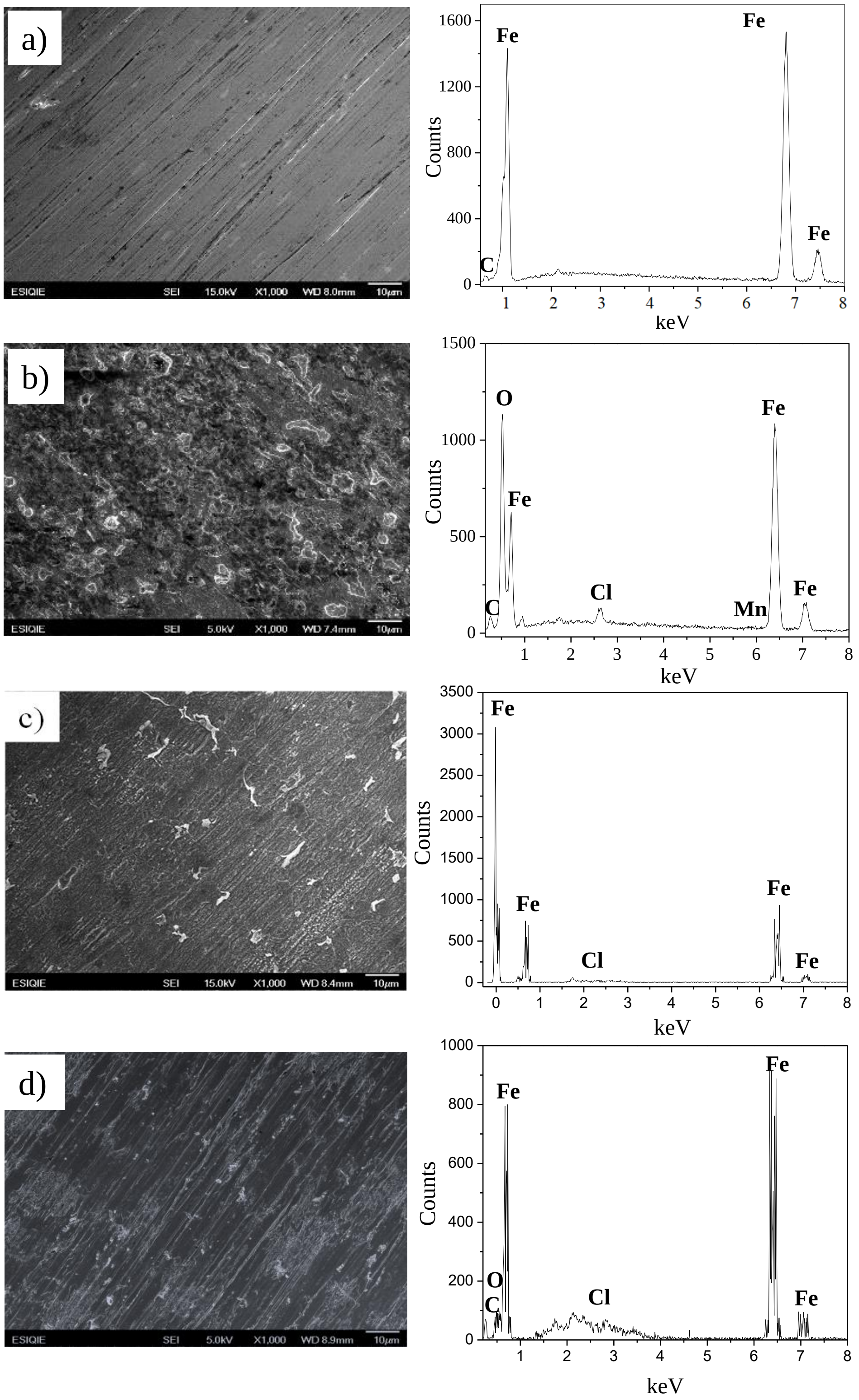

Figure 6. Micrographs and EDS of a) steel API 5L X52 before the immersion test, b) after 24 h immersion in 0.5 M HCl, c) after 24 h immersion in 0.5 M HCl and 100 ppm $(HEMIM)^+ (CN)^-$ and d) after 24 h immersion in 0.5 M HCl and 5 ppm $(DMIM)^+ (Cl)^-$ at 25 ° C.

The surfaces of the API 5L X52 steel before and after the corrosion processes, in the absence and presence of 100 ppm of the (HEMIM)$^+$ (CN)$^-$ and 5 ppm of the (DMIM)$^+$ (Cl)$^-$ after 24 h of immersion at 25 °C, were observed by SEM. Figure 6a depicts the micrographs of the API 5L X52 steel surface before immersion in the acid, observing a surface free of corrosion products and the characteristic scratch lines of the sample preparation. The corresponding EDS presents in greater proportion the characteristic peaks of the Fe. Figure 6b shows the surface steel after 24 h of immersion in the corrosive medium in the absence of inhibitor, revealing a damaged surface due to the dissolution of the metal and the formation of corrosion products (FeClOH and FeOOH) [26,27]. Meanwhile, Figure 6c, obtained in the presence of (HEMIM)$^+$ (CN)$^-$, exhibits lesser damage than in the absence of the inhibitor (Figure 6a) and still, the scratch lines and some pitting are observed. In the presence of (DMIM)$^+$ (Cl)$^-$, Figure 6d, the characteristic lines of the mechanical grinding are also observed, and the damage is even smaller. Therefore, in the presence of the ILs, the corrosion is smaller compared to that of the sample without IL, giving evidence of the adsorption of the IL molecules and demonstrating their effectiveness.

3.3.2 AFM

The AFM technique is one of the most powerful techniques for observing surface topography [28,29]. Figure 7 shows the high-resolution and three-dimensional images obtained for the API 5L X52 steel in the absence and presence of the compounds (HEMIM)$^+$ (CN)$^-$ and (DMIM)$^+$ (Cl)$^-$ at 25 ° C. Figure 7a shows the morphology of the surface of the API 5L X52 in absence of the CI, observing a severely corroded surface topography, due to the oxidation reaction responsible for the dissolution of the metal and also the presence of corrosion products. In the figures 7b and 7c, it can be observed that the surfaces in the presence of 100 ppm of the (HEMIM)$^+$ (CN)$^-$ and 5 ppm of the (DMIM)$^+$ (Cl)$^-$ in comparison with that of the target, are less rough due to the minor corrosive attack.

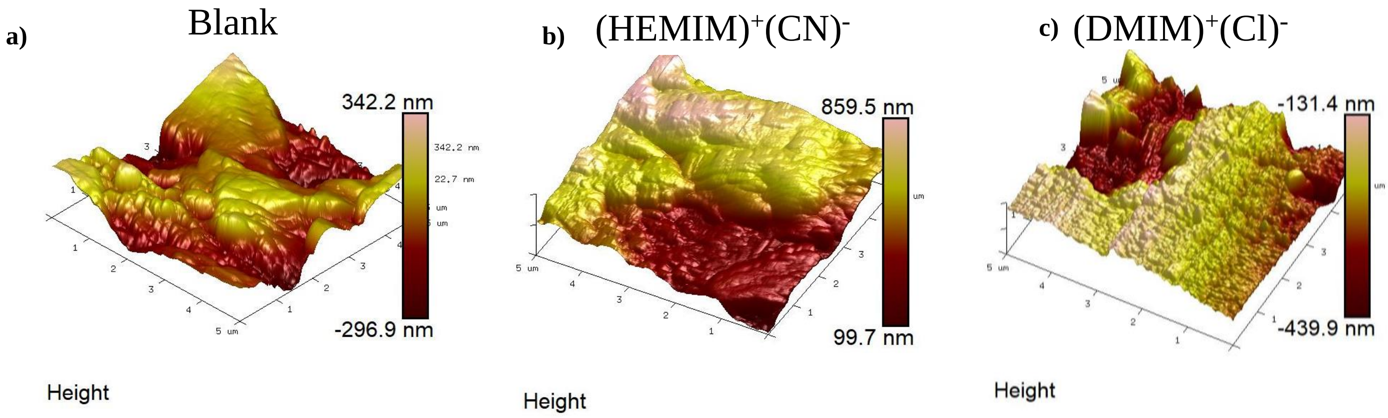

Figure 7. AFM images obtained for API 5L X52 steel in a) 0.5 M HCl, b) 0.5 M HCl + 100 ppm (HEMIM)$^+$ (CN)$^-$ and c) 0.5 M + 5 ppm (DMIM)$^+$ (Cl)$^-$.

The average surface roughness (R_a) in the absence and presence of the corrosion inhibitors were calculated. It is evident that the values of R_a in the absence of inhibitor are higher (84.9 nm) compared to the values in the presence of the molecules of (HEMIM)$^+$ (CN)$^-$, 64.6 nm, and (DMIM)$^+$ (Cl)$^-$, 45.6 nm. The presence of the IL reduces the roughness by 24 and 46 %, respectively. This reduction in the R_a

is attributed to the formation of the inhibitor film on the surface of the steel, which allowed to reduce the effect of corrosion. However, it is evident that in sites not blocked by IL, the process of pitting corrosion still occurs, as was observed by MEB, however, the degree of coverage and performance of the IL is favorable. These results confirm what was observed by the electrochemical and gravimetric techniques, the adsorption of the inhibitor on the surface and consequently the inhibition of the corrosion process.

3.4 Solution analyses

3.4.1 Ultraviolet-visible spectroscopy (UV-vis)

UV-vis spectroscopy is a powerful tool that is employed to provide evidence of the interaction between a metal and a CI. Figure 8 shows the UV-vis adsorption spectra in the wavelength range of 200 to 400 nm, obtained in the 0.5 M HCl solution in the presence of 100 and 5 ppm of the $(HEMIM)^+$ $(CN)^-$ and the $(DMIM)^+$ $(Cl)^-$, respectively, before and after exposing the steel samples for 24 h. The spectra obtained show in both cases bands in the UV-vis region associated with transitions of type $n \rightarrow \pi^*$ and $\pi \rightarrow \pi^*$, attributed to the π electrons of the imidazolium group. In the presence of the IL, a decrease in the bands is observed, which could be due to the interaction between IL and steel [30].

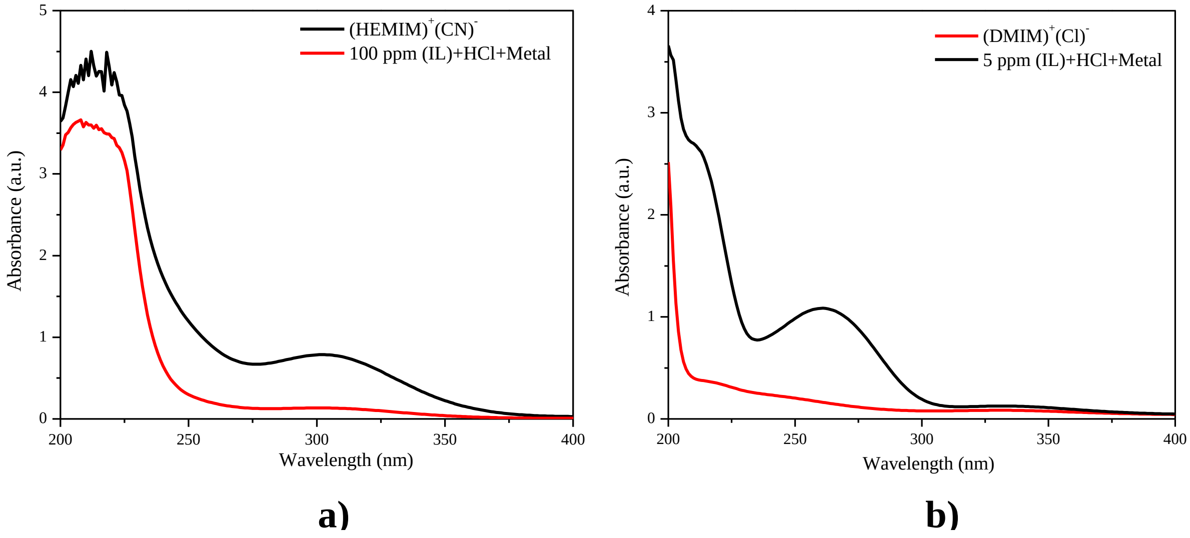

Figure 8. UV-Vis spectra of the IL a) $(EMIM)^+$ $(CN)^-$ and b) $(DMIM)^+$ $(Cl)^-$ before and after 24 h immersion in 5 ppm in 0.5 M HCl at 25 °C.

3.5 Adsorption isotherm

The nature of the process between the inhibitor and the metal surface can be studied by fitting the adsorption isotherms [31]. The coverage degree of the inhibitor (θ) is related to % *EI* by:

$$\theta = \frac{\% EI}{100} \qquad (10)$$

where θ are the zones occupied by the IC, while (θ - 1) corresponds to the presence of active sites on the surface of the metal. Under this criterion, there are different models of isotherms that allow establishing the physical/chemical characteristics of the metal/solution interface. The Langmuir, Frumkin, Freundlich, and Temkin isotherms are adsorption models that have been used to describe the interaction of adsorbed molecules on the metal surface [32].

Considering the % EI_{PP} obtained by the potentiodynamic polarization technique, adjustments were made with the models described above and the best fit obtained was with the Langmuir isotherm model (Figure 9) for both inhibitors, with correlation coefficients, R^2 of 0.9792 and 0.999, respectively.

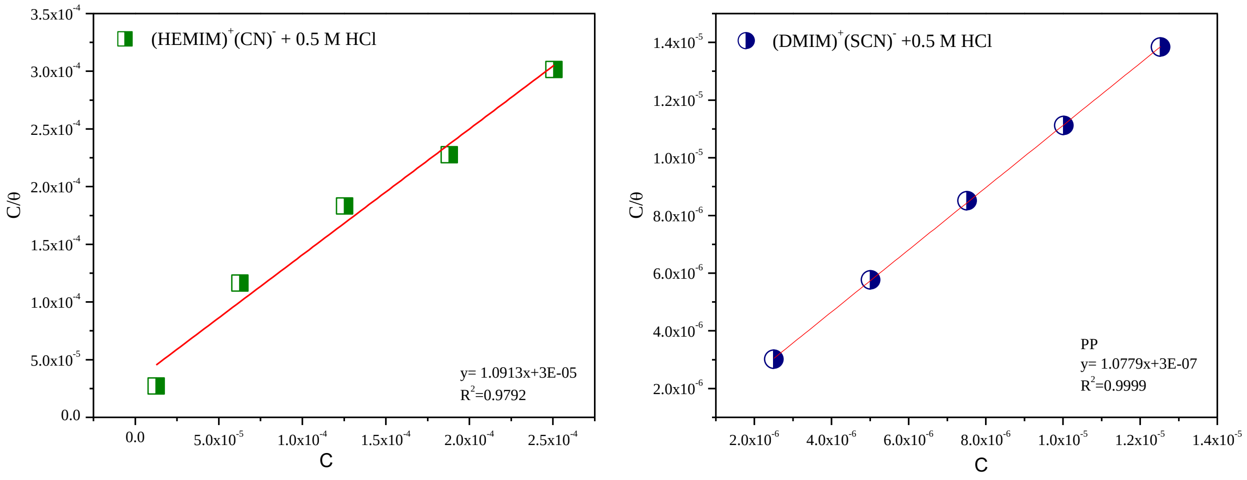

a) **b)**

Figure 9. Langmuir type adsorption isotherm for API 5L X52 steel in the presence of a) $(HEMIM)^+ (CN)^-$ and b) $(DMIM)^+ (Cl)^-$ in 0.5 M HCl medium.

The following equation was used for the adjustment:

$$\frac{C}{\theta} = \frac{1}{K_{ads}} + C \qquad (11)$$

where K_{ads} is the equilibrium constant of adsorption and C the concentration of the inhibitor. The K_{ads} values were calculated from the reciprocal of the intersection of the straight line and are shown in Table 6. Considering that the K_{ads} values indicate the adsorption strength of the molecules, it is evident that the $(DMIM)^+ (Cl)^-$ is more strongly adsorbed on the metal surface compared to the compound $(HEMIM)^+ (CN)^-$.

Table 6. Thermodynamic parameters of adsorption of API 5L X52 steel in the presence of ILs in a 0.5 M HCl solution.

System	K_{ads} x 10^{-2} (mol^{-1})	$-\Delta G^{\circ}_{ads}$ (kJ mol^{-1})
$(HEMIM)^+ (CN)^-$ /0.5 M HCl	330	35.77
$(DMIM)^+ (Cl)^-$ /0.5 M HCl	3300	45.08

Once the adsorption isotherm was established, the free adsorption energy (ΔG°_{ads}) was calculated using the following equation:

$$\Delta G^{\circ}_{ads} = -RTln(55.5K_{ads}) \qquad (12)$$

where $\Delta G^{\circ}_{\text{ads}}$ is the standard free energy of adsorption, *R* is the gas constant (J mol^{-1} K^{-1}), *T* is the temperature (K), and the value of 55.5 is the concentration of water in the solution expressed in mol. The negative values of $\Delta G^{\circ}_{\text{ads}}$ guarantee the spontaneity of the adsorption process and the stability of the film adsorbed on the metal surface [33]. Table 7 shows the values obtained from $\Delta G^{\circ}_{\text{ads}}$ for each IL at 25 °C. It has been reported that values of $\Delta G^{\circ}_{\text{ads}}$ above -20 kJ mol^{-1} are associated with physical interaction processes, that is, an electrostatic-type interaction like the Van Der Waals forces, corresponding to a physisorption; if the values are greater than -40 kJ mol^{-1} associate to a chemical adsorption involving an electron transfer between the inhibitor molecules and the metal surface, to form a coordination bond, corresponding to a chemisorption [34]. The value of $\Delta G^{\circ}_{\text{ads}}$ calculated for the $(\text{HEMIM})^{+}$ $(\text{CN})^{-}$ was 35.77 kJ mol^{-1} and for the $(\text{DMIM})^{+}$ $(\text{Cl})^{-}$ of 45.08 kJ mol^{-1}, so the ILs are fundamentally chemisorbed on the surface of the steel. It is important to note that the $(\text{DMIM})^{+}$ $(\text{Cl})^{-}$ has a higher adsorption strength even at low concentrations.

3.6 Theoretical calculations

Quantum chemistry calculations were performed to establish the relationship between the experimental inhibition efficiencies and the quantum parameters of the IL. Initially, the IL molecules were optimized in such a way as to avoid the presence of too large or small link lengths or angles, thus obtaining more stable structures and in a lower energy state [35,36]. The optimized structures are shown in Figure 10. The geometric state of the ILs as well as the nature of their molecular orbital boundaries: HOMO (occupied molecular orbital of higher energy) and LUMO (unoccupied molecular orbital of lower energy) were calculated. The HOMO gives information about the possible sites or regions in the inhibitor molecule where the most free-electron is probably donated to free orbitals of the metal atoms, while LUMO shows the sites or regions in the IL molecules where the electron of the occupied orbitals can be back-donated (Figure 10).

Figure 10 shows that the LUMOs of the ILs are located in the imidazolium ring and the HOMOs in the chain. It is evident that the $(\text{DMIM})^{+}$ $(\text{Cl})^{-}$ has more adsorption sites than the $(\text{HEMIM})^{+}$ $(\text{CN})^{-}$, therefore, so it could have a greater adsorption capacity. [37,38]. Some parameters such as E_{HOMO}, E_{LUMO}, the energy band (ΔE), the ionization potential (*I*), electron affinity (*A*), global hardness (η), softness (σ), dipole moment (μ) and the fraction of transferred electrons (ΔN) obtained by quantum calculations and equations (1-4) are shown in Table 8. E_{HOMO} values are generally associated with the molecule's ability to donate electrons [39, 40]. Therefore, high values of E_{HOMO} indicate a strong tendency of the molecule to donate electrons. The results obtained show that $(\text{HEMIM})^{+}$ $(\text{CN})^{-}$ presents the slightly higher values of E_{HOMO}. Thus, $(\text{HEMIM})^{+}$ $(\text{CN})^{-}$ has a higher tendency to give electrons to the metal surface and therefore, tend to adsorb more strongly. While low values of E_{LUMO}, are associated with the ability of the molecule to accept electrons, the results indicate that the $(\text{DMIM})^{+}$ $(\text{Cl})^{-}$ can accept electrons more easily than the $(\text{HEMIM})^{+}$ $(\text{CN})^{-}$ [41]. Molecules with a high value of ΔE are more stable; however, they present a low reactivity, while molecules with low values are generally more polarizable and can adsorb more easily on the metal surface. Given the values obtained, both molecules would exhibit good adsorption properties, which confirm the experimental inhibition efficiencies obtained.

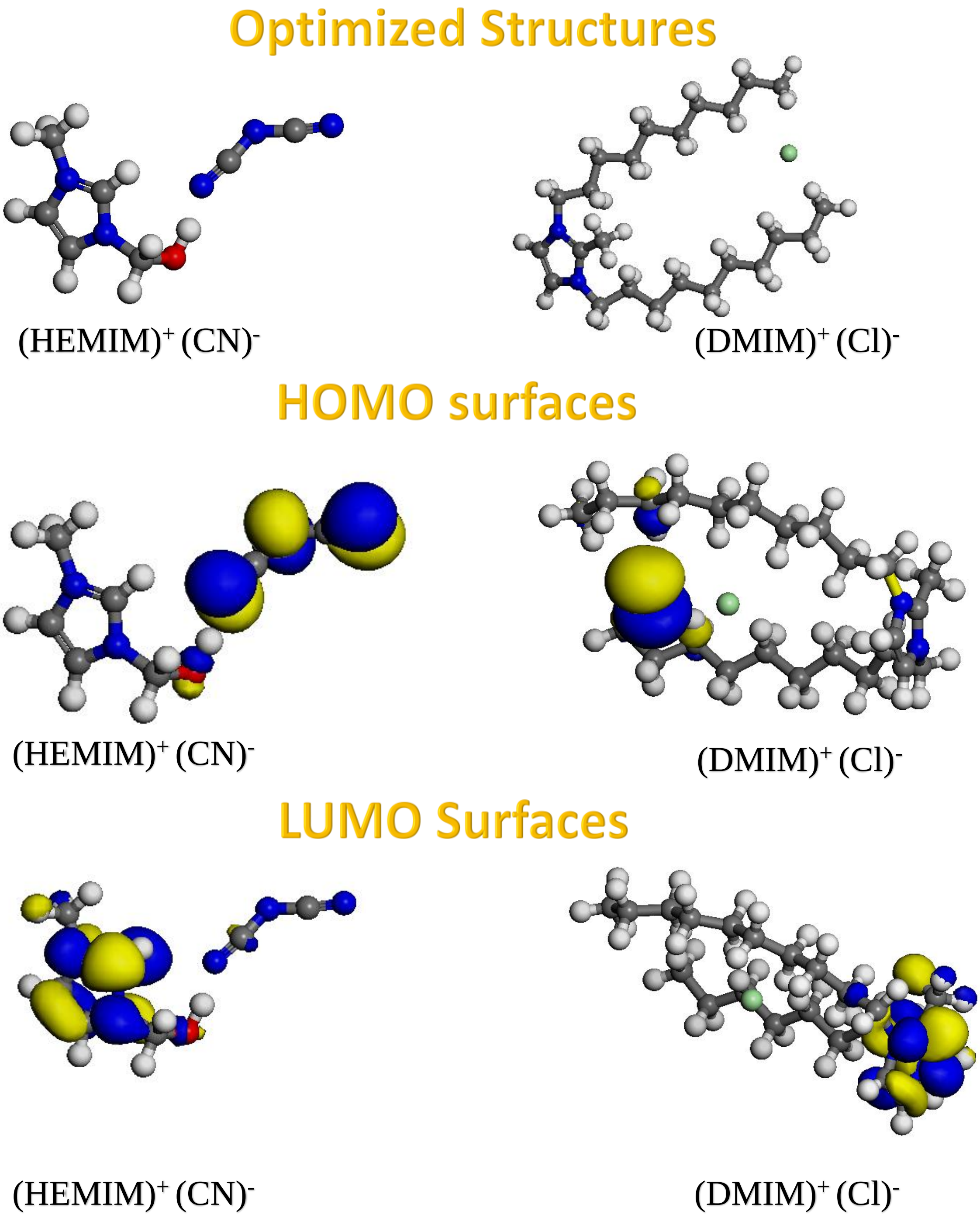

Figure 10. Optimized structures, HOMO and LUMO for the IL $(HEMIM)^+$ $(CN)^-$ and $(DMIM)^+$ $(Cl)^-$.

The hardness (η) and the softness (σ) are parameters that can also be related to the efficiency of inhibition based on the acid-base theory [42]. A hard molecule has a high value of η and therefore a low value in σ, while a soft molecule has a lower hardness. [43]. Soft molecules could more easily offer electrons than hard molecules, so greater adsorption could occur in molecules whose value of σ is bigger. The values reported in Table 7 show that the $(DMIM)^+$ $(Cl)^-$ has the highest values of σ so it would tend to adsorb more easily to the metal surface. Another parameter that allows to establish the type of adsorption is the dipole moment (μ), molecules with a high value of μ tend to form strong interactions between the molecule and the metal through dipole-dipole bonds, promoting strong adsorption and therefore a good inhibition efficiency [44]. The obtained values show that both molecules present a good value of μ, corroborating the high efficiencies obtained experimentally.

Table 7. Quantum chemical parameters calculated for each IL.

Parameters	$(HEMIM)^+ (CN)^-$	$(DMIM)^+ (Cl)^-$
E_{HOMO} (eV)	-5.53	-4.84
E_{LUMO} (eV)	-1.69	-2.01
ΔE (eV)	3.84	2.84
Dipole moment (μ)	16.7	16.6
Ionization potential, *I* (eV)	5.53	4.84
Electron afinity, *A* (eV)	1.69	2.01
Hardness, η	1.92	1.41
Softness, *σ*	0.52	0.70

The electronic properties allow us to know many of the properties by which the molecules could perform as good inhibitors of corrosion. However, they are not enough to predict the tendency and the yield of inhibition, so it is necessary to know more directly the interaction of the CI with the surface of the steel in the presence of water to simulate a real medium. For this, a simulation was performed under the Monte Carlo method, and the values obtained are presented in Table 8. It is evident that the adsorption energy of the $(DMIM)^+ (Cl)^-$ is higher than that of the $(HEMIM)^+ (CN)^-$ supporting the best experimentally efficiency for the $(DMIM)^+ (Cl)^-$. The adsorption energies of IL are higher than that of water molecules, thus indicating the possibility of a gradual replacement of water molecules with IL molecules, with the consequent formation of a protective film on the surface of the metal and high efficiency of inhibition.

Table 8. Parameters calculated from the Monte Carlo simulation for the adsorption of $(HEMIM)^+ (CN)^-$ and $(DMIM)^+ (Cl)^-$ on Fe (110) / 50 molecules of H_2O (in Kcal mol^{-1})

Inhibitor	Plane	Total Energy	Adsorption Energy	Rigid Adsorption Energy	Deformation Energy	Inhibitor dE_{ad}/dN_i	Water dE_{ad}/dN_i
$(HEMIM)^+ (CN)^-$	110	-1372.8	-1445.6	-1388.9	-56.6	-147.2	-13.9
$(DMIM)^+ (Cl)^-$	110	-1452.6	-1696.4	-1478.4	-32.9	-456.9	-13.7

It has been established that the adsorption of an inhibitor at the metal/solution interface depends mainly on the chemical structure and charge distribution of the molecule and the nature and charge of the metal [45]. Since the surface of the steel in acid medium presents a positive charge, it facilitates in the case that the acid is the HCl the adsorption not only of the water molecules but also of the chloride ions and with it the surface acquires an excess of negative charges [46]. This excess of negative charges on the surface favors the adsorption of the cation of both ILs: $(HEMIM)^+$ and $(DMIM)^+$, by electrostatic attraction. On the other hand, the ILs are chemically adsorbed due to the formation of coordination bonds between the pair of free electrons of the N^+ atoms (Figure 11) present in the molecules of the ILs and the empty orbitals of the Fe atoms, improving the stability and efficiency of inhibition. According to the values of ΔG°_{ads} calculated, it is evident that the process mostly occurs through the chemisorption of the ILs. In some studies [47], it has been demonstrated that the IL anion can be adsorbed in the positively charged sites of the metal. Under this consideration, it is possible the adsorption of both: cation and anion, on the surface of the steel, for both ILs, as shown in Figure 11.

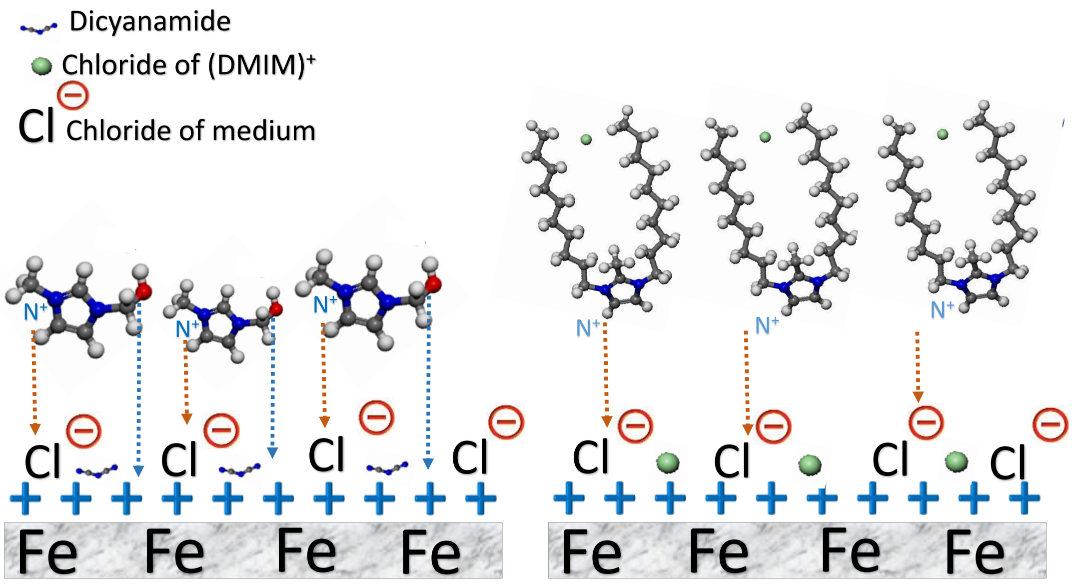

a) **b)**

Figure 11. Mechanism of inhibition proposed for API 5L X52 steel in the presence of: a) $(HEMIM)^+$ $(CN)^-$ and b) $(DMIM)^+$ $(Cl)^-$ and HCl.

In the case of $(DMIM)^+$ $(Cl)^-$ after the formation of the first monolayer, the formation of multilayers stabilized by Van der Waals forces between the alkyl chain and the adsorbed molecule can occur [48]. The presence of this long chain allows the formation of a more compact film at the metal/solution interface, which would explain that this compound has a higher efficiency of inhibition at low concentrations and that it is more stable at high temperatures.

Table 9 shows the comparative performance of the ILs evaluated in this study with other ILs that have been reported as corrosion inhibitors in HCl medium on the carbon steel surface. It is observed that all the ILs are shared as a mixed type inhibitor, the type of adsorption obey Langmuir isotherm, and physical and chemical adsorption processes occur. It is important to note that for the ILs reported it is necessary to add IL concentrations > 100 ppm for to obtain efficiencies in the order of 80 - 98 %, while for the case of $(DMIM)^+$ $(Cl)^-$, only 5 ppm was necessary to reach an efficiency of 91%. The best performance of the $(DMIM)^+$ $(Cl)^-$ could be due that its adsorption occurs only through chemisorption process (ΔG°_{ads} = -45.08 kJ mol^{-1}) and the presence of an alkyl chain that acts as a barrier between the corrosive medium and the metal surface [49].

Table 9. ILs as corrosion inhibitors for mild steel in HCl medium, mode of absorption and techniques used for the evaluation performance.

Inhibitor	Medium	Techniques	Performance	Reference
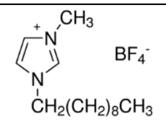 1-decyl-3-methylimidazolium tetrafluoroborate $(C_{10}MIM)^+(BF_4)^-$	1 M HCl	Electrochemical, spectroscopic techniques Quantum chemical calculations Quantitative structure-activity relationship (QSAR) Monte Carlo simulations	500 ppm 98.08 % *IE* Mixed-type inhibitor Langmuir isotherm ΔG^0_{ads} = - 36.64 $kJmol^{-1}$	[49]
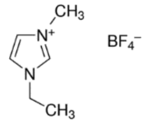 1-ethyl-3-methylimidazolium tetrafluoroborate $(BMIM)BF_4$	1 M HCl	Electrochemical, spectroscopic techniques Quantum chemical calculations Monte Carlo simulation	500 ppm 77.93 % *IE* Mixed-type inhibitor Langmuir isotherm. ΔG^0_{ads} = - 33.70 $kJmol^{-1}$	[50]
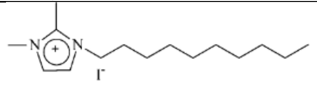 1,2-dimethyl-3-decylimidazole iodide (DDI)	1 M HCl	Electrochemical and spectroscopic techiniques	100 ppm 67 % *IE* Mixed-type inhibitor Frumkin isotherm. ΔG^0_{ads} = -8.7 $kJmol^{-1}$	[51]
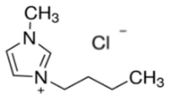 1-butyl-3-methylimidazolium chlorides (BMIC)	1 M HCl	Gravimetrical and electrochemical techniques	1750 ppm 87.5 % *IE* Mixed-type inhibitor Langmuir isotherm ΔG^0_{ads} = - 27.3 $kJmol^{-1}$	[52]
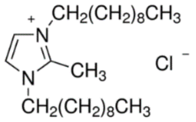 1,3-didecyl-2-methylimidazolium chloride $(DMIM)^+ (Cl)^-$	0.5 M HCl	Gravimetric, electrochemical, and spectroscopic techniques Quantum chemical calculations Monte Carlo simulation	5 ppm 90.9 % *IE* Mixed-type inhibitor Langmuir isotherm. ΔG^0_{ads} = -45.08 $kJmol^{-1}$	In this study
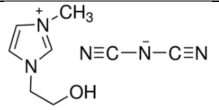 1-(2-hydroxyethyl)-3-methylimidazolium dicyanamide $(HEMIM)^+ (CN)^-$	0.5 M HCl	Gravimetric, electrochemical, and spectroscopic techniques Quantum chemical calculations Monte Carlo simulation	100 ppm 83.2 % *IE* Mixed-type inhibitor Langmuir isotherm. ΔG^0_{ads} = -35.77 $kJmol^{-1}$	In this study

4. CONCLUSIONS

The ionic liquids 1-(2-Hydroxyethyl)-3-methylimidazolium dicyanamide $(HEMIM)^+ (CN)^-$ and 1,3-Didecyl-2-methylimidazolium chloride $(DMIM)^+ (Cl)^-$ are efficient inhibitors of corrosion of API 5L X52 steel in HCl 0.5M. The % EI increases with the increase in the concentration of the IL but decreases with the increase in temperature due to the increase in the iron oxidation reaction and desorption of the IL cation adsorbed on the steel surface. In the presence of 100 ppm of $(HEMIM)^+ (CN)^-$ and 5 ppm of $(DMIM)^+ (Cl)^-$, maximum efficiencies of 92 and 97% were obtained, respectively. It was determined that the ILs are mixed type inhibitors and that their adsorption on the surface of the metal obeys to a Langmuir type adsorption isotherm. The values of the K_{ads} and ΔG°_{ads} indicate that the ILs are strongly chemisorbed on the surface of the metal and that the presence of the alkyl chain allows the formation of a more compact layer, so it presents a better performance even at lower concentration (5 ppm). UV-vis studies revealed chemical interactions between metal and IL. Theoretical results agree with those obtained experimentally, suggesting that both molecules have good adsorption energy, however, the $(DMIM)^+$ $(Cl)^-$ presented the best molecular and experimental properties, due to the presence of the alkyl chain that serves as a barrier of corrosive spaces in the metal/solution interface.

ACKNOWLEDGEMENT
M. C. L. would like to thank CONACyT for the Ph.D. scholarship granted. The authors also like to thank SIP-IPN project 20181031, and BEIFI-IPN scholarship. E.M.A.E. and T. L. M., thank the SNI for the distinction of the membership and the stipend received.

References

1. M. Goyal, S. Kumar, I. Bahadur, C. Verma and E.E. Ebenso, *J. Mol. Liq*., 256 (2018) 565.
2. M. Askari, M. Aliofkhazraei, S. Ghaffari and A. Hajizadeh*, J. Nat. Gas. Sci. Eng*., 58 (2018) 92.
3. V. Rajeswari, D. Kesavanb, M. Gopiramanc, P. Viswanathamurthi, K. Poonkuzhali and T. Palvannan, *Appl. Surf. Sci*., 314 (2014) 537.
4. N.A. Negm, Y.M. Elkholy, M.K. Zahran and S.M. Tawfik, *Corros. Sci*., 52 (2010) 3523.
5. A. Rochdi, O. Kassou, N. Dkhireche, R. Touir, M. El Bakri, M. EbnTouhami, M. Sfaira, B. Mernari and B. Hammoutid, *Corros. Sci*., 80 (2014) 442.
6. H.A. Sorkhabu and M. Es΄haghi, *Mater. Chem. Phys*., 114 (2009) 267.
7. G. Vastag, A. Shaban, M. Vraneš, A. Tot, S. Belić and S. Gadžurić, *J. Mol. Liq*., 264 (2018) 526.
8. P.A. Lozada, O.Olivares Xometl, N.V. Likhanova, I.V. Lijanova, J.R.V. García and R.E.H. Ramírez, *J. Mol. Liq*., 265 (2018) 151.
9. A.H. Nahlé, T.J. Harvey and F.C. Walsh, *J. Alloys Compd*., 765 (2018) 812.
10. E. Ituen, O. Akaranta and A. James, *J. King. Saud Univ. Eng. Sci*., https://doi.org/10.1016/j.jksues.2017.07.002
11. U. Domańska, P. Papis and J. Szydlowski, *J. Chem. Thermodyn*., 77 (2014) 63.
12. Y. Guo, B. Xu, Y. Liu, W. Yang, X. Yin, Y. Chen, J. Le and Z. Chen, *J. Ind. Eng. Chem.*, 56 (2017) 234.
13. A.M.E. Shamy, K. Zakaria, M.A. Abbas and S.Z.E. Abedin, *J. Mol. Liq*., 211 (2015) 363.
14. N.V. Likhanova, M.A. Domínguez-Aguilar, O. Olivares-Xometl, N. Nava-Entzana, E.M. Arce and H. Dorantes, *Corros. Sci*., 52 (2010) 2088.
15. H. Bentrah, Y. Rahali and A. Chala, *Corros. Sci*., 82 (2014) 426.
16. F. Bentiss, M. Traisnel, H. Traisnel, H.F. Hildebrand and M. Lagrenee, *Corros. Sci*., 46 (2004) 2781.
17. F. Bentiss, M. Lebrini and M. Lagrenée, *Corros. Sci*., 47 (2005) 2915.
18. S. John, A. Joseph, T. Sajini and J.J. Ajith, *Egypt J. Petrol*., 26 (2016) 721.
19. I. Lozano, E. Mazario, C.O. Olivares-Xometl, N.V. Likhanova and P. Herrasti, *Mater. Chem. Phys*., 147 (2014) 191.
20. M. Yadav, D. Behera and S. Kumar, *Surf. Interface Anal*., 46 (2014) 640.
21. H. Keleş, *Mater. Chem. Phys*., 130 (2011) 1317.
22. Y. Tang, X. Yang, W. Yang, R. Wan, Y. Chen and X. Yin, *Corros. Sci*., 52 (2010) 1801.
23. C.H. Hsu and F. Mansfeld, *Corrosion*, 57 (2001) 747.
24. M. Tourabi, K. Nohair, M. Traisnel, C. Jama and F. Bentiss, *Corros. Sci*., 75 (2013) 123.
25. R. Macdonald and D.R. Franceshetti, Impedance Spectroscopy, 1987, Wiley, New York.
26. E.A. Noor and A.H. Al-Moubaraki, *Int. J. Electrochem. Sci*., 3 (2008) 806.
27. A.K. Satapathy, G. Gunasekaran, S.C. Sahoo, K. Amit and P.V. Rodrigues, *Corros. Sci*., 51 (2009) 2848.
28. R. Solmaz, *Corros. Sci*., 81 (2014) 75.
29. G. Kardas, M. Çulha, B. Yazıcı and M. Erbil, *Electrochim. Acta*, 53 (2008) 5941.

30. M Yadav, S Kumar, I Bahadur and D. Ramjugernath, *Int. J. Electrochem Sci*., 9 (2014) 6529.
31. I. Ahamad, R. Prasad and M.A. Quraishi, *Corros. Sci*., 52 (2010) 933.
32. J. Tan, L. Guo and S. Xu, *J. Ind. Eng. Chem*., 25 (2015) 295.
33. M. Bouklah, B. Hammouti, M. Lagrenée and F. Bentiss, *Corros. Sci*., 48 (2006) 2831.
34. F. El-Hajjaji, M. Messali, A. Aljuhani, M.R. Aouad, B. Hammaouti, M.E. Belghiti, D.S. Chauhan and M.A. Quraishi, *J. Mol. Liq*., 249 (2018) 997.
35. F. Bentiss, M. Traisnel, H. Vezin and M. Lagrenée, *Corros. Sci*., 46 (2003) 371.
36. D. Zhang, L. Gao and G. Zhou, *Corros. Sci*., 46 (2004) 3031.
37. W. Li, Q. He, C. Pei and B. Hou, *Electrochim. Acta*, 52 (2007) 6386.
38. I.B. Obot, S.A. Umoren, Z.M. Gasem, R. Suleiman and B. El Ali, *Ind. Eng. Chem*., 21 (2015) 1328.
39. E.E. Ebenso, M.M. Kabanda, L.C. Murulana, A.K. Singh and S.K. Shukla, *Ind. Eng. Chem. Res*., 51 (2012) 12940.
40. M.M. Kabanda, S.K. Shukla, A.K. Singh, L.C. Murulana and E.E. Ebenso, Int. J. *Electrochem. Sci*., 7 (2012) 8813.
41. Z.Y. Cao, Y.M. Tang, H. Cang, J.Q. Xu, G. Lu and W.H. Jing, *Corros. Sci*. 83 (2014) 292.
42. R.G. Pearson, Proc. *Natl. Acad. Sci., U.S.A*. 83 (1986) 8440.
43. M.M. Kabanda, L.C. Murulana, M. Ozcan, F. Karadag, I. Dehri, I.B. Obot, and E.E. Ebenso, *Int. J. Electrochem. Sci*., 7 (2012) 5035.
44. N.O. Obi-Egbedi and I.B. Obot, *Corros. Sci*., 53 (2011) 263.
45. A. Fouda, M. Ismail, G. E. Elewady and A. Abousalem, *J. Mol. Liq*., 240 (2017) 372.
46. K. Bhrara, H. Kim and G. Singh, *Corros. Sci*., 50 (2008) 2747.
47. S. Yesudass, L. O. Olasunkanmi, I. Bahadur, M. M. Kabanda, I.B. Obot and E. E. Ebenso, *J. Taiwan Inst. Chem. Eng*., 64 (2016) 252.
48. L. Feng, S. Zhang, Y. Qiang, S. Xu and B. Tan, *Mater. Chem. Phys*., 215 (2018) 229.
49. Y. Sasikumar, A.S. Adekunle, L.O. Olasunkanmi, I. Bahadur, R. Baskar, M.M. Kabanda, I.B. Obot and E.E. Ebenso, *J. Mol. Liq*., 211 (2015) 105-118.
50. X. Zhou, H. Yang and F. Wang, *Electrochim. Acta,* 56 (2011) 4268.
51. O. Olivares-Xometl, C. López-Aguilar, P. Herrastí-González, N.V. Likhanova, I. Lijanova, R. Martínez-Palou and J. A. Rivera-Márquez, *Ind. Eng. Chem. Res*., 53 (2014) 9534.
52. Q.B. Zhang and Y.X. Hua, *Electochim. Acta*, 54 (2009) 1881.